Article:
Panda, SK, Dash, SK, Bhaskaran, B et al. (1 more author) (2016) Investigation of the snow-monsoon relationship in a warming atmosphere using Hadley Centre climate model. Global and Planetary Change, 147. pp. 125-136. ISSN 0921-8181

https://doi.org/10.1016/j.gloplacha.2016.10.013

Investigation of the Snow-Monsoon Relationship in a Warming Atmosphere Using Hadley Centre Climate Model

S. K. Panda[a], S. K. Dash[a], B. Bhaskaran[b,*], and K. C. Pattnayak[a]

[a]Centre for Atmospheric Sciences
Indian Institute of Technology Delhi
Hauz Khas, New Delhi -110 016, India

[b]Met Office Hadley Centre
FitzRoy Road, Exeter, EX1 3PB, UK

* Current Affiliation:
Fujitsu Laboratories of Europe
Hayes Park Central, Hayes
Middlesex, UK

Corresponding Address

Dr. Subrat Kumar Panda
Centre for Atmospheric Sciences
Indian Institute of Technology Delhi
Hauz Khas, New Delhi -110 016, India
Tel: +91 11 2659 6023
Fax: +91 2659 1386
E-mail: subrat75@gmail.com

Abstract

Several studies based on observed data and models show that there is an inverse relationship between the strength of the Indian summer monsoon and the extent/depth of Eurasian snow in the preceding season. Perturbed Physics Ensemble (PPE) simulations of HadCM3 have been used in this study to re-examine the snow-monsoon relationship in the longer time scale. The PPE monthly precipitation values during June, July, August and September (JJAS) have been compared with the corresponding values of Climatic Research Unit (CRU) for the period 1961-1990. The PPEs which simulated the Indian Summer monsoon reasonably well have been used for examining snow-monsoon relationship. Atmospheric fields such as wind, geopotential height, velocity potential and stream function from the PPE simulations have been examined in detail. Results show that because of the west Eurasian snow depth anomalies, the mid-latitude circulation undergoes significant changes, which in turn lead to weak/strong monsoon circulation during deficient/excess Indian Summer Monsoon Rainfall (ISMR) respectively. The first Empirical Orthogonal Function (EOF1) of winter snow depth for the period 1961-1900 over the whole of Eurasia explains 13% variability. Thus the significant correlation patterns are consistent with the most dominant EOF of snow depth, in which the first mode describes a dipole type structure as observed. The study confirms that snow depth in the western part of Eurasia (20^0E-65^0E and 45^0N-65^0N) has negative correlation with the ISMR.

Keywords: Indian Summer Monsoon Rainfall (ISMR), Perturbed Physics Ensemble (PPE), Empirical Orthogonal Function (EOF1)

1. Introduction

The summer monsoon rainfall over the Indian sub-continent is found to be more significant in terms of its space and time variability. The Indian summer monsoon (also known as southwest monsoon) contributes about 80% of the annual rainfall over most parts of the country during the four months from June to September, while Tamil Nadu receives maximum rainfall during winter monsoon. Indian summer monsoon is part of a seasonally reversing wind system characterized by wet summers and dry winters. The wind during summer monsoon season are associated with a large scale vorticity at 850 hPa and the Low Level westerly Jet (LLJ) over the Arabian Sea and an anticyclone (the Tibetan anticyclone) at the upper level (200 hPa) with the monsoon easterly jet. The economical progress of the country is mostly dependent on the behavior and changes in summer monsoon precipitation. Dash et al. (2012) examined the characteristics of extreme precipitation and temperature events during the Indian summer monsoon months with 9-member ensembles over the period 1982 to 2009 using RegCM3. Their study shows that, the simulated extreme weather conditions like very wet days, extremely wet days, warm days and warm nights are more often as compared to those in India Meteorological Department (IMD) observed values in Central India. Ashfaq et al. (2009) simulated the dynamical features of the summer monsoon with 25 km resolution over South Asia region and found that enhanced greenhouse forcing resulted in the overall suppression of summer monsoon precipitation, delay in onset and an increase in the occurrence of monsoon break periods.

Long back Blanford (1884) suggested that the varying extent and thickness of continental snow cover exerts an influence on the land surface's thermal characteristics and in turn, influences the onset of the Asian summer monsoon. Because continental snow cover in the Asian region persists for a long time and snow-monsoon relationship is observed to be inverse, it has remained as one of the important parameters in empirical long range prediction of monsoon. Studies of Hahn and Shukla (1976), Kripalani and Kulkarni (1999), Bamzai and Shukla (1999), **Fasullo (2004)** based on observed data emphasized on the inverse relationship between the Indian Summer Monsoon Rainfall (ISMR) and the Eurasian snow cover/depth in the preceding season. Kripalani et al. (2003) further reiterated that the summer monsoon over India and south Asia are primarily governed by large-scale atmospheric features like ENSO and Eurasian winter snow cover.

Barnett et al. (1989), Yasunari et al. (1991) and Vernekar et al. (1995) used a number of General Circulation Models (GCM) to examine and analyses the relationship between snow and monsoon. Their results clearly indicate that a positive snow anomaly over Eurasia in winter/spring does affect the monsoon circulation in the following summer in terms of weaker monsoon. Sankar-Rao et al. (1996) using data from National Environmental Satellite Data and Information Service (NESDIS) of the National Oceanic and Atmospheric Administration (NOAA) for the period 1967 to 1992 concluded that following the winters of more snow, stationary perturbations with higher pressures over central Asia north of India are produced in the lower atmosphere and the following Asian summer monsoon is weaker. Simultaneously, in the upper-atmosphere, lower anomalous pressure occurs during summer which weakens the upper level monsoon high.

Dash et al. (2004, 2005) tried to show the impact of Eurasian snow depth anomalies on the Indian summer monsoon rainfall anomaly through the mid-latitude circulations. They used Soviet snow depth data and Indian rainfall data for the period 1951-1994 and showed that in winter through spring undergo significant changes in the upper and lower level winds, geopotential height, velocity potential and stream function fields. Such changes in the large-scale circulation pattern may be interpreted as precursors to weak/strong monsoon circulation and deficient/excess ISMR. Dash et al. (2006a) confirmed the inverse snow-ISMR relationship by using the actual observed values of snow depth of Historical Soviet Daily Snow Depth (HSDSD) version II data set in the spectral GCM of IITD. The Regional Climate Model version 3 (RegCM3) has also been integrated from 1st April to 30th September in four years (Dash et al. 2006b, Shekhar and Dash 2005) starting from 1993. Monthly snow depth data based on NIMBUS-7 SMMR satellite are used for conducting sensitivity experiments with RegCM3. Their simulations reveal that excess Tibetan snow in April decreases the rainfall over India in the following monsoon season. Their simulations also show that lower level westerlies and upper level easterlies are weakened in the snow experiment than in the control experiment.

From the global warming point of view relation between Eurasian snow and ISMR is an important issue, some studies in the recent past show changes in the characteristics of summer monsoon rainfall in the warming atmosphere. The robust inverse relationship between Eurasian snow and ISMR is essential to be examined in the warming atmosphere. PPE simulations of Hadley Centre, UK Met Office have provided data over a large number of years and hence the objective of this study is to use those model scenarios to

examine above. CRU rainfall data have been used for comparison. The PPEs which give better results in terms of ISMR have been selected for the study of snow monsoon relationship in a warming scenario. Finally, the characteristics of upper and lower-level mean monsoon circulations and midlatitude circulations during extreme snow depths years over Eurasia will also be examined in detail. The description of model details and selection of PPEs has been described in Section 2. Section 3 discusses the results, while summary and conclusions are given in the last Section 4.

2. Description of the Model and Simulations

2.1. Model Details

The PPE simulations are made mainly on an ensemble of variants of the slab version of HadCM3. HadCM3 is the third generation Hadley Centre model of UK Met Office. It is a coupled atmosphere-ocean GCM developed at the Hadley Centre and described by Gordon et al. (2000). The atmospheric component of the model has 19 levels with a horizontal resolution of 2.5 degrees of latitude by 3.75 degrees of longitude, which produces a global grid of 96 x 73 grid cells.). The governing equations are solved using a semi explicit finite difference scheme at 30 minute interval. More details of the formulation and climate of the atmosphere component of the model can be found in Pope et al. (2000). The oceanic component of the model has 20 levels with a horizontal resolution of 1.25 degrees of latitude by 1.25 degrees of longitude.

2.2. Simulation Details and Description of PPEs

Perturbed Physics Ensemble (PPE) is mainly based on an ensemble of variants of the slab version of the HadCM3, mainly where variations are generated by changing the

values of the input parameters those control physical processes. It provides a new approach in which modeling uncertainties are sampled systematically by perturbing known but uncertain parameters. As per Stainforth et al. (2005) PPE identifies a set of model variants which samples the settings of multiple uncertain parameters according to prior distributions estimated by experts based on their knowledge of the relevant physical processes. The PPE method represents an attempt to develop a systematic method of sampling modeling uncertainties within a single model framework. The most thorough way to investigate this uncertainty is to run a massive ensemble experiment in which each relevant parameter combination is investigated. Its main advantage is that it allows greater control over the design of experiments to sample process uncertainties.

A recent study by Murphy et al. (2007) shows that the probabilistic predictions of future climate change is based on a set of ensemble simulations of equilibrium and time dependent changes, carried out by perturbing poorly constraints parameters controlling key physical and biogeochemical processes in the HadCM3 coupled ocean-atmosphere global climate model These experiments allow quantification of the effects of earth system modeling uncertainties and internal climate variability of feedbacks likely to exert a significant influence on twenty-first century climate at regional scales. Parameters were perturbed in the atmosphere and sea-ice components in order to generate the ensemble and sample the uncertainties in climate feedback processes.

PPEs were performed with CO_2 levels set at pre-industrial and double pre-industrial levels. In Murphy et al. (2004), each of the 53 ensemble members was generated by perturbing atmosphere, sea ice or land-surface parameters away from their standard value or by switching on and off particular options within a parameterisation

scheme. Using the 53 experiments with single parameter perturbations the effects of multiple parameter perturbations to the model could be inferred from a linear combination of the output from those runs. From those output, they picked 128 versions by splitting the resultant distribution of climate sensitivity into 64 equally probable bins and picking 20 model versions from each bin with the best **Climate Prediction Index (CPI)** score. Taking this 1280 subset of the four million, and starting from the model version with the best CPI score, then they picked the model that was furthest away from that version as measured by a non-dimensional measure of distance in model parameter space. The 128 model versions were run in slab configuration. They also picked 16 versions to run contemporaneously in fully coupled configuration by taking the parameter settings with the best predicted CPI score in the subset of eight model versions from four adjacent climate sensitivity bins. Again, the aim was to sampling a wide range of (predicted) sensitivities and parameter values from the 128 member slab model ensemble.

A new 17-member PPE of HadCM3 transient simulations (denoted by PPE_A1B) has recently been produced, in order to provide user-relevant predictions of twenty-first century climate change. These are driven from 1860 to 2000 by historical time series of well-mixed GHGs, ozone, anthropogenic sulphur emissions and reconstructions of variations in solar activity and volcanic aerosol and from 2000 to 2100 by future GHG concentrations and sulphur emissions from the SRES A1B scenario (Nakicenovic & Swart 2000). One ensemble member uses standard parameter settings, with 16 perturbed members chosen from the parameter combinations used by Webb et al. (2006). These were selected by choosing the member with the best simulation of present-day climate, followed by 15 further members designed to maximize a non-dimensional measure of the

average distance between members in terms of both climate sensitivity and model parameter values.

3. Results

3.1. Simulated Indian Summer Monsoon in PPEs

Indian summer monsoon circulation along with the accompanied rainfall is one of the most important atmospheric phenomena which needs to be tested by a GCM. Hence, in this study some of the important meteorological variables such as precipitation, wind at both 850 hPa & 200hPa and surface temperature from the 17 PPE simulations are used for the period 1961 to 1990 in order to examine the main characteristics on Indian summer monsoon. For this study, Climatic Research Unit (CRU) rainfall data from 1961 to 1990 has been used for the validation of model.

The time series of ISMR averaged for the period 1860-2098 over all the Indian land points have been depicted in Figure 1 for all the PPEs. The thick line in the middle indicates the mean of all the PPEs. In this figure, the summation of mean and standard deviation are depicted above the thick line and the difference between mean and standard deviation are depicted below the thick line. The figure indicates increase in ISMR after around 2000. Mean, Standard Deviation (SD) and Coefficient of Variation (CV) of summer monsoon rainfall are shown in Figure 2a, b and c respectively during the period 1961-1990. Figure 2a shows that rainfall is more over the west coast, north east and Bay of Bengal. Mean PPEs (Figure 2a) simulated rainfall spatial distribution depicts that JJAS mean rainfall are about 10-12 mm/day over the Northeast India, 8-12 mm/day over the East Coast, 8-10 mm/day over the West Coast and 6-8 mm/day over the Northwest India.

Thus the mean PPEs is able to capture the major rainfall regions over India. Figure 2b show that the standard deviations of summer monsoon rainfall simulated by mean PPEs are 3.5 mm/day, 2.5 mm/day and 1.5 mm/day over the North east, East coast and West Coast of India respectively. Figure 2c explains CV over North east, East coast and West Coast of India are 35%, 25% and 20% respectively. PPE monthly precipitation values during June, July, August and September (JJAS) have been compared with the corresponding values from CRU for the period 1961-1990. First the mean PPE JJAS precipitation have been regridded with respect to those of CRU and then applied an Indian mask in the PPE simulations and CRU. The differences between each regridded PPE and CRU are depicted in Figure 3. **The PPEs such as 0, 2, 4, 7, 8, 13, 14 and 15 has overestimated the rainfall over east coast and north east part of India by 2-3 mm/day compared with the CRU rainfall. These PPEs underestimates the simulated rainfall over the plains of Central India and Rajasthan by 2-3 mm/day. Another group of PPEs such as 1, 3, 5, 6, 9, 10, 11, 12 and 16 has overestimated the rainfall over southern Peninsular by 2-3 mm/day. These groups of PPEs are not able capture the rainfall over the central India. These PPEs underestimates 1-3 mm/day rainfall over the northern and north east of India.** The Root Mean Square Errors (RMSE), pattern correlations and standard deviations between PPE and CRU rainfall have been examined to select which PPEs result are better representation of observed ISMR. Figure 4 shows that there are two groups of PPEs out of which one gives better result in terms of high pattern correlation and less RMSE. The group consists of 0, 2, 4, 7, 8, 13, 14 and 15 members is selected for snow-monsoon study.

3.2. Snow Monsoon Relationship in PPEs

Based on the above results, the first groups are used for examining snow-monsoon relationship. When entire period of 1860 to 2098 is considered. Figure 5 shows the ensemble mean of **December, January and February (DJF)** Eurasian snow-depth and ISMR standardised anomalies are inversely related. Spatial patterns of correlation coefficients depicted in Figure 6a show two dominant modes. Thus DJF snow depth over western Eurasia has negative correlation while those over eastern Eurasia have positive correlation with the subsequent ISMR. EOFs of winter (DJF) snow depth for the period 1961–1990 have also been computed for the western part of Eurasia. It is found that EOF-1 over the western Eurasia explains about 13% of variability as shown in Figure 6b. Hence the significant correlation patterns are consistent with the most dominant EOF of snow depth, in which the first mode describes a dipole type structure.

3.3. Categorization of Snow and Monsoon Years:

Using the monthly snow depth data for the years 1861–2008, DJF mean values for each year in west Eurasia are computed along with the mean of the series and the standard deviations. The snow depth is expressed as a standardized snow-depth anomaly by dividing the variations of each year from its normal value by the standard deviation. The standardized snow-depth anomaly thus calculated over west Eurasia for the period 1861–2008 is shown by solid line with open circle in Figure 7. The years with snow-depth anomaly between ±0.5 standard deviations are considered as normal snow years. Similarly, the years with snow-depth anomaly above +0.5 standard deviation are counted

as high snow years and those with less than –0.5 standard deviation snow depth anomaly are identified as low snow years. In order to increase the sample size, the classification based on ±0.5 standard deviation is adopted here. The ISMR anomaly for each year has also been computed and plotted using the solid line with closed circle in Figure 7. Following the criterion of IMD, the years having ISMR anomaly more than +1 standard deviation (above 90% of its long-term average value) are termed as excess monsoon years and those less than –1 standard deviation are considered deficient monsoon years. The years with an ISMR anomaly between –1 and +1 standard deviations are classified as normal monsoon years. We have selected the years 1888, 1913, 1959 and 1976 are high snow years and 1867, 1923, 1964 and 1989 are low snow years.

3.4. Characteristics of Circulations in the extreme snow-monsoon years:

Bamzai and Shukla (1999) emphasized that the inverse snow-monsoon relationship holds especially in those years when snow is anomalously high or low for both the winter as well as the consecutive spring season. If there is heavy snow cover in winter it is likely that it will affect the snow cover in spring. Heavy snow cover in midwinter usually does not easily melt because of low-level solar insolation. If there is already snow on the ground, the precipitation in February, March and in April is likely to be in the form of snow (because of the surface temperature close to 0°C) rather than rain. Such a process could explain the results of Bamzai and Shukla (1999). Hence, to examine the evolution of the mean monsoon fields a season in advance in response to the snow depth over west Eurasia, the two groups of extreme snow and ISMR years are selected. The difference in the circulation characteristics in high snow (1888, 1913, 1959 and

1976) and low snow (1867, 1923, 1964 and 1989) years are studied in detail by analyzing the composite difference fields of wind, geopotential height, stream function and velocity potential in the mean of JJAS separately.

3.4.1 Winds

The wind differences (m/s) between the composites of high and low snow years at 850 hPa and 200hPa are shown in Figure 8 for the monsoon season. Figure 8a indicates that a well-organized anomalous cyclonic circulation over central Eurasia. There is an anomalous westerly to the south of Caspian Sea, which implies that the westerly is stronger in the high snow depth case than in the low snow depth case. There is indication of an anomalous anticyclonic circulation over the north Arabian sea and west India centred at about 20°N and 75°E which contributes to the anomalous easterlies over the Arabian Sea during JJAS. This implies that Asian summer monsoon lower-level westerlies are weaker in response to high Eurasian snow depth than in low snow depth. Most of India affected by the anomalous anticyclonic circulation during monsoon season at the lower level (Figure 8a) results in a weak monsoon circulation in high snow compared to low snow years. From the examination of the upper level (200 hPa) (Figure 8b) wind difference fields in JJAS, a well-developed anomalous anticyclonic circulation is found over southeast Asia in high snow years compared to low snow years. An anomalous anticyclonic circulation is shown over central Eurasia and an anomalous weak anticyclonic circulation is simulated over Bay of Bengal and south east Asia. It seems that such anomalous features suppress the development of upper tropospheric anticyclones and hence the monsoon circulations over India. These results indicate that Asian summer monsoon easterlies are weaker in response to high snow depth than in

snow depths are less. The anomalous winds at the upper level correspond to weaker easterlies in the deficient monsoon years in response to high snow compared to the excess rain years. It also shows that during the year of high snow, the easterlies started weakening to give rise to weak monsoon upper level easterlies during JJAS. Also in JJAS, anomalous westerlies are found over the South China Sea. Such anomalous westerlies during high snow years arrest the north northwest movement of the Tibetan anticyclone from its winter position over the equator to its summer position over Tibet. Such anomalous features suppress the development of upper tropospheric anticyclones and hence the monsoonal circulation over India.

3.4.2 Geo-potential Height

The geo-potential height difference (m) between composites of high and low snow years field in JJAS are shown in Figures 9a at the lower troposphere and in Figure 9b at the upper troposphere. The negative difference fields over the western Eurasia in Figure 5.12a can be attributed to the higher snow. From, Figure 9a it is seen that the monsoon heat low over central south Asia is weaker (positive values) in high snow years compared to low snow years. This positive geo-potential difference field indicates an adverse pressure gradient anomaly in winter which persists through spring up to the monsoon season. The geo-potential difference field at 200 hPa in Figure 9b indicates a weaker upper level high (negative values) over west Eurasia and east Asia in JJAS. Such lower anomalous pressure at the upper level covering the entire region from the middle latitudes in Asia to India was reported by Sankar-Rao et al. (1996).

3.4.3 Velocity Potential

It is well known that there is a strong upper level divergent centre associated with the Asian monsoon. The correlations between the monsoon rainfall and 200-hPa velocity potential, a good surrogate for the "Walker circulation," are strong in the period 1958-80 (Kumar et al., 1999). The differential heating leads to the growth of available potential energy which is next passed on to the divergent motions via the covariance of vertical velocity and temperature. The final link in this scenario is the transfer of energy from the divergent to the rotational part of the motion field that describes the monsoon. These are largely described by *and* χ interaction (where is a stream function and χ is a velocity potential) Krishnamurti et al. (1998).

The lower and upper level seasonal tropospheric velocity potential difference between composites of high and low snow years in JJAS are shown in Figures 10a and b. It is well known that there is a strong upper level divergent center (Krishnamurti, 1972) associated with the Asian monsoon. At 850 hPa (Figure 10a) the negative values over Indian subcontinent are prominent which gives a weaker convergence of monsoon. The positive difference fields over the Indian subcontinent and the negative difference fields to the east in Figure 10b indicate that the upper level divergence center was weaker over India in high snow years compared to low snow. This divergent circulation changed in such a way that the intensity of easterlies over the monsoon regions of southern Asia and Africa was weak in high snow years. In their study Chen and van Loon (1987) have inferred that the anomalous divergent circulation during years of weak tropical easterly jet reduces the generation of kinetic energy on the upstream side of the jet and the

destruction of kinetic energy on the downstream side of the jet. From this figure, it may be noticed that there is a dipole structure in the form of divergence and convergence centers over Indian subcontinent and east of India. Analysis of velocity potential difference fields both at the upper and lower levels yields that the upper level divergence/convergence centers have their corresponding convergence/divergence centers in the lower level.

3.4.4. Stream Function

Large-scale divergence and convergence are analyzed with velocity potential, and non-divergence component of wind is monitored with stream function. The stream function differences (m^2/s) between composites of high and low snow years at the lower and upper level troposphere are shown in Figures 11(a) and (b). The formation of negative stream function in the upper troposphere (200hPa), the negative is stronger over north India region and as well as over west Eurasia. Based on this analysis it may be inferred that weakening of the upper level circulation over India in the high snow years in JJAS.

4. Conclusions

The PPE simulations of Hadley Centre, UK Met Office have been used to examine the relationship between winter snow depth anomalies over Eurasia and ISMR anomalies. By and large the model simulates the ISMR satisfactorily. The snow depth in the western part of Eurasia is found to have negative correlation with ISMR. EOF1 of winter snow depth for the period 1961-1990 over the whole of Eurasia explains 13% variability. Hence the significant correlation patterns are consistent with the most dominant EOF of

snow depth, in which the first mode describes a dipole type structure. Atmospheric fields such as wind, geopotential height, velocity potential and stream function from the simulations are examined in detail to study the influence of Eurasian snow on the monsoon circulation. Wind fields show that in the years of high snow, upper level easterlies weakens and gives rise to weak monsoon. During the monsoon time anomalous westerlies are found over the South China Sea. Such anomalous westerlies during high snow years arrest the north northwest movement of the Tibetan anticyclone from its winter position over the equator to its summer position over Tibet. Such anomalous features suppress the development of upper tropospheric anticyclones and hence the monsoonal circulation over India. The geopotential height fields at lower levels show that the monsoon heat low over central south Asia is weaker in the high snow years compared to the low snow years. The geo-potential difference indicates weaker upper level high over west Eurasia and India. Finally the study concludes that even in the warming atmosphere the inverse relationship between the depth of Eurasian and ISMR holds good.

Acknowledgements

This paper is the outcome of UK-India collaborative research. Dr. S. K. Panda is thankful UKMO and British Council, New Delhi for supporting his visit to UKMO. The authors are thankful to Dr. Saroj Kanta Mishra for his valuable suggestion and help for giving some input to the text.

References

Bamzai, A.S., Shukla, J., 1999. Relation between Eurasian Snow Cover, Snow Depth and the Indian summer monsoon: An observational study. J Clim 12, 3117–3132.

Barnett, T.P., Dumenil, L., Schlese, U., Roeckner, E., Latif, M., 1989. The effect of Eurasian snow over on regional and global climate variations. J Atmos Sci 46, 661–685.

Blanford, H.F., 1884. On the connection of the Himalaya snowfall with dry winds and seasons of drought in India. Proc Roy Soc London 37,3–22.

Dash, S.K., Singh, G.P., Vernekar, A.D., Shekhar, M.S., 2004. A study on the number of snow days over Eurasia, Indian rainfall and seasonal circulations. Meteor Atmos Phys 86,1-13.

Dash, S.K., Singh, G.P., Shekhar, M.S., Vernekar, A.D., 2005. Response of the Indian summer monsoon circulation and rainfall to seasonal snow depth anomaly over Eurasia. Clim Dyn 24,1–10.

Dash, S.K., Sarthi, P.P., Panda, S.K., 2006a. A study on the effect of Eurasian snow on the summer monsoon circulation and rainfall using a spectral GCM. Int J Climatol 26,1017-1025.

Dash, S.K., Shekhar, M.S., Singh, G.P., 2006b. Simulation of Indian summer monsoon circulation and rainfall using RegCM3. Theor Appl Climatol 86,161-172.

Fasullo, J., 2004. A stratified diagnosis of the Indian monsoon-Eurasian snow cover relationship. J. Clim 17, 1110-1122.

Hahn, D.J., Shukla, J., 1976. An apparent relation between Eurasian snow cover and Indian monsoon rainfall. J Atmos Sci, 33,2461–2462.

Kripalani, R.H., Kulkarni, A., 1999. Climatology and variability of historical Soviet snow depth data: some new perspectives in snow – Indian monsoon tele-connection. J Atmos Sci 15,475–489.

Kripalani, R.H., Kulkarni, A., Sabde, S.S., Khandekar, M.L., 2003. Indian Monsoon variability in a global warming scenario. Nat. Hazards 29,189-206.

Murphy, J., et al. 2004. Quantification of modelling uncertainties in a large ensemble of climate change simulations. Nature 430,768–772.

Murphy, J. et al., 2007. A methodology for probabilistic predictions of regional climate change from perturbed physics ensembles. Philos Trans Roy Soc London A365,1993-2028.

Nakicenovic, N., Swart, R., 2000. Special report on emissions scenarios. Cambridge, UK, Cambridge University Press.

Sankar-Rao, M., Lau, M.K., Yang, S., 1996. On the relationship between Eurasian snow cover and the Asian summer monsoon. Int J Climatol 16,605–616.

Shekhar, M.S., Dash, S.K., 2005. Effect of Tibetan spring snow on the Indian summer monsoon circulation and associated rainfall. Curr Sci India 88 (11),1840-1844.

Stainforth, D.A., et al., 2005. Uncertainity in prediction of the climate response to rising levels of greenhouse gases. Nature 433:403-406, doi:10.1038/nature03301.

Vernekar, A.D., Zhou, J., Shukla, J., 1995. The effect of Eurasian snow cover on the Indian monsoon. J Clim 8,248–266.

Webb et al., 2006. On the contribution of local feedback mechanisms to the range of climate sensitivity in two GCM ensembles. Clim Dyn 27,17–38, doi:10.1007/s00382-006-0111-2.

Yasunari, T., Kitoh, A., Tokioka, T., 1991. Local and remote responses to excessive snow mass over Eurasia appearing in the northern spring and summer climate-a study with MRI GCM. J Meteor. Soc. Japan 69,473-487.

Figure Captions

Fig. 1. Time series of simulated ISMR averaged over the Indian land for the period 1860-2098.

Fig. 2. Simulated ISMR for the period 1961-1990: (a) mean, (b) Standard deviation, and (c) Coefficient of variation.

Fig. 3. Difference in ISMR between the individual PPE and CRU for the period 1961-1990.

Fig. 4. (a) The Root Mean Square Error (RMSE), and (b) pattern correlation of 17 PPE. (c) RMSE versus pattern correlation, and (d) RMSE versus standard deviation between 17 PPE and CRU precipitations for the period 1961-1990.

Fig. 5. Standardized DJF snow depth anomalies over western Eurasia (open circles) and ISMR anomalies (closed circles) during 1861–2098.

Fig. 6. (a) Correlation coefficients between DJF Eurasian snow depth anomalies with the following ISMR anomalies during 1961-1990 and (b) EOF-1(13%) of DJF snow depth during 1961-1990.

Fig. 7. Standardized DJF snow depth anomalies over western Eurasia (open circles) and ISMR anomalies (closed circles) during 1861–2008.

Fig. 8. Geopotential height differences (m) between composites of high and low snow years at (a) 850 hPa level and (b) 200 hPa.

Fig. 9. Geopotential height differences (m) between composites of high and low snow years at (a) 850 hPa level and (b) 200 hPa.

Fig. 10. Velocity potential (χ) differences (m^2/s) between composites of high and low snow years at (a) 850 hPa and (b) 200 hPa.

Fig. 11. Stream function differences (m^2/s) between composites of high and low snow years at (a) 850 hPa and (b) 200 hPa.

Figures

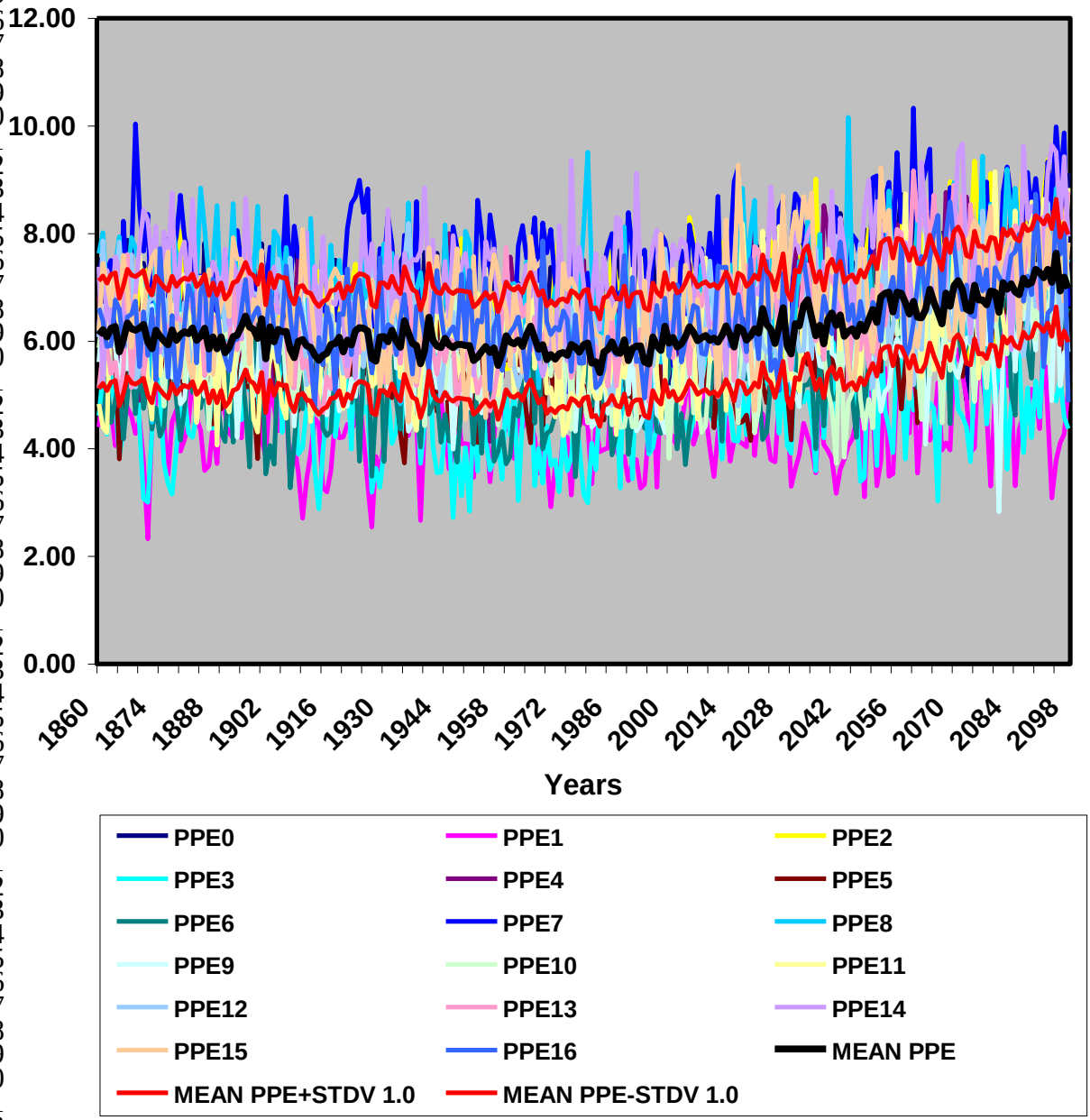

Figure 1: Time series of simulated summer monsoon rainfall (mm/day) averaged over the Indian land for the period 1860-2098.

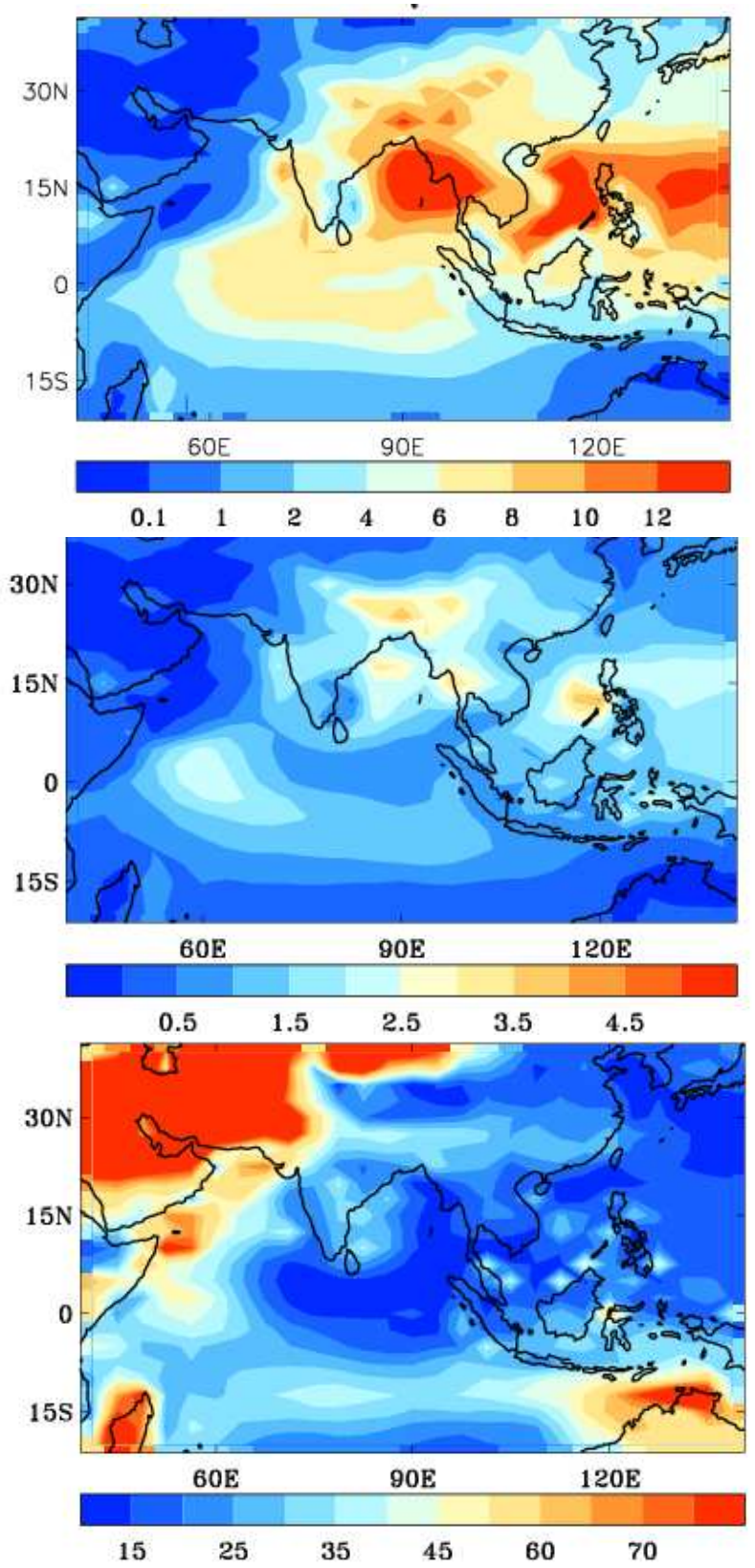

Figure 2: Simulated Indian summer monsoon rainfall for the period 1961-1990: (a) mean, (b) Standard deviation, and (c) Coefficient of variation.

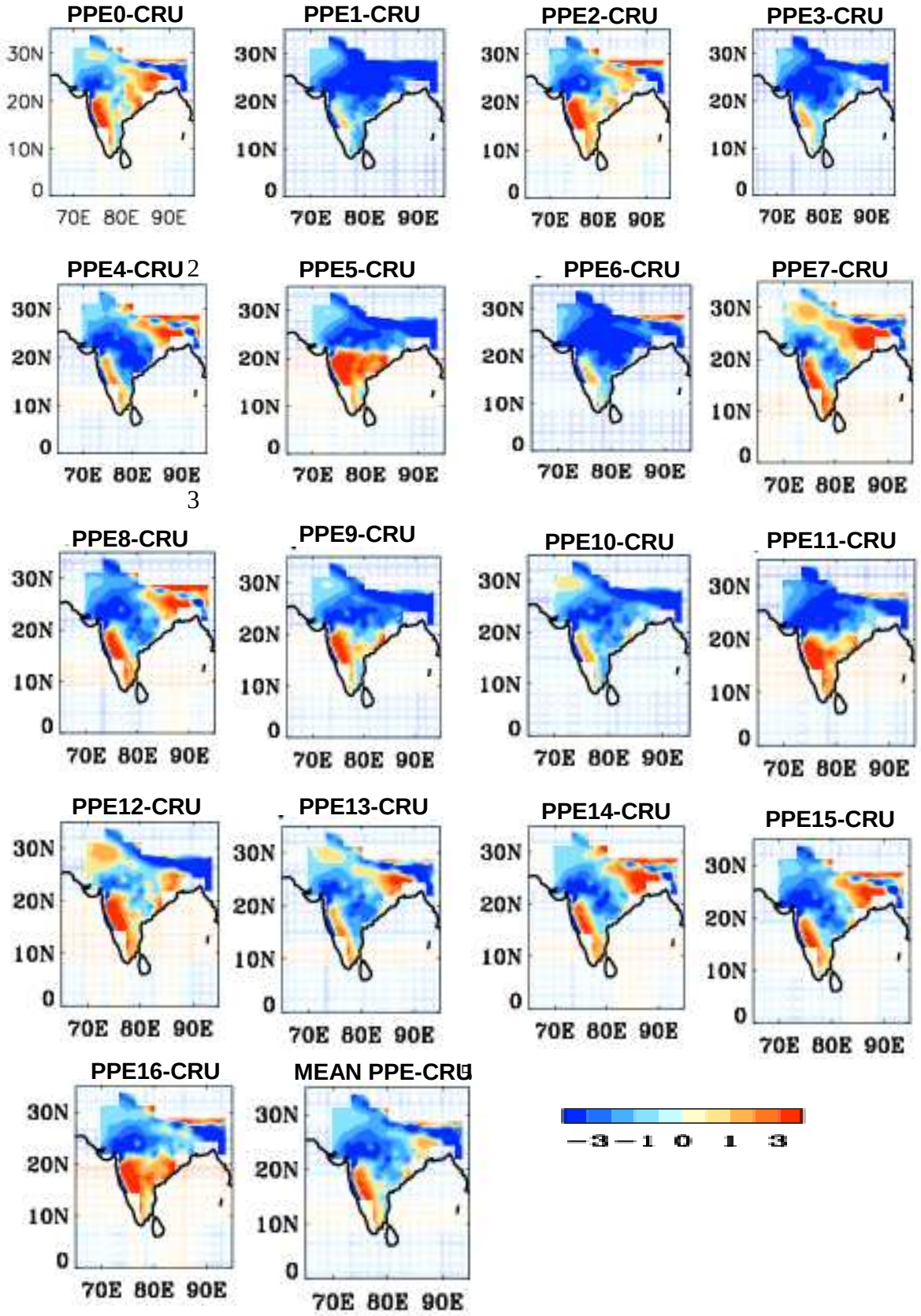

Figure 3: Difference in Indian summer monsoon rainfall between the individual PPE and CRU for the period 1961-1990.

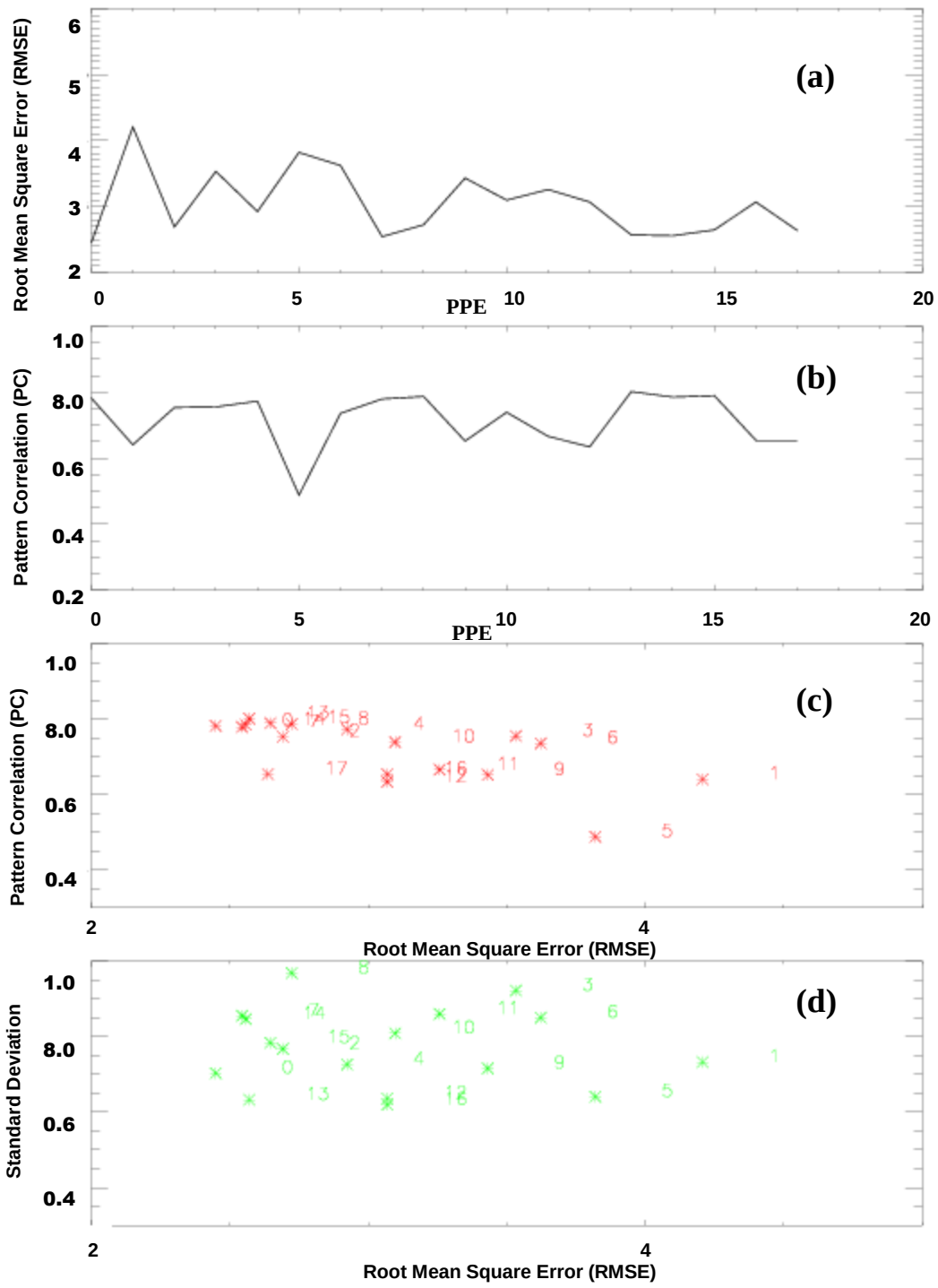

Figure 4: (a) The Root Mean Square Error (RMSE), and (b) pattern correlation of 17 PPE. (c) RMSE versus pattern correlation, and (d) RMSE versus standard deviation between 17 PPE and CRU precipitations for the period 1961-1990.

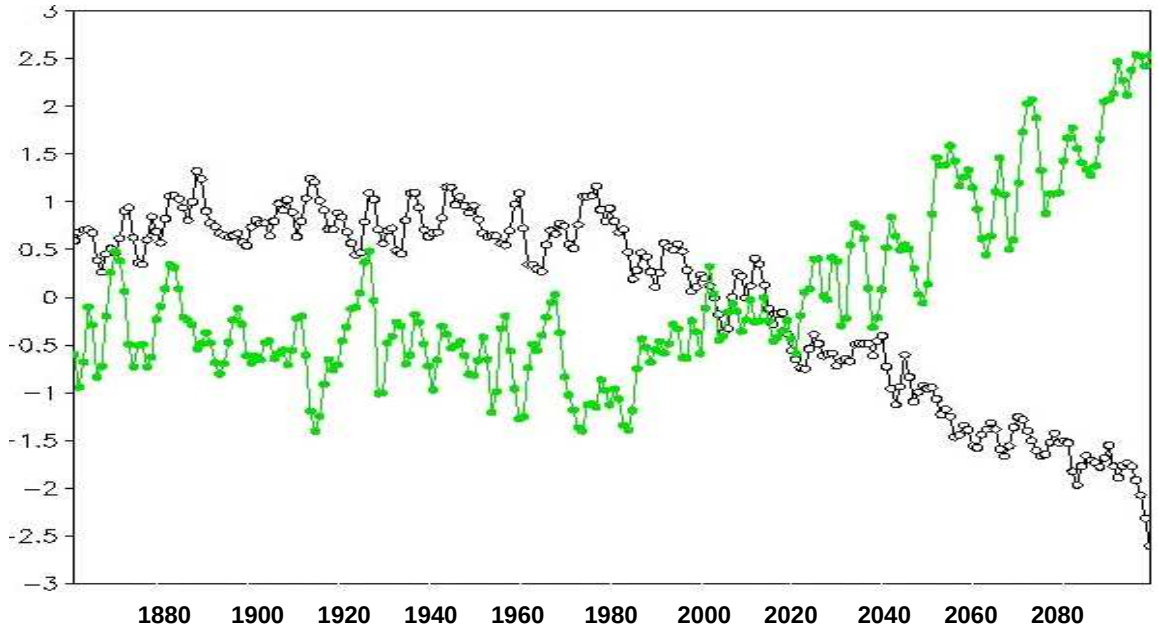

Figure 5: Standardized DJF snow depth anomalies over western Eurasia (open circles) and ISMR anomalies (closed circles) during 1861–2098.

1

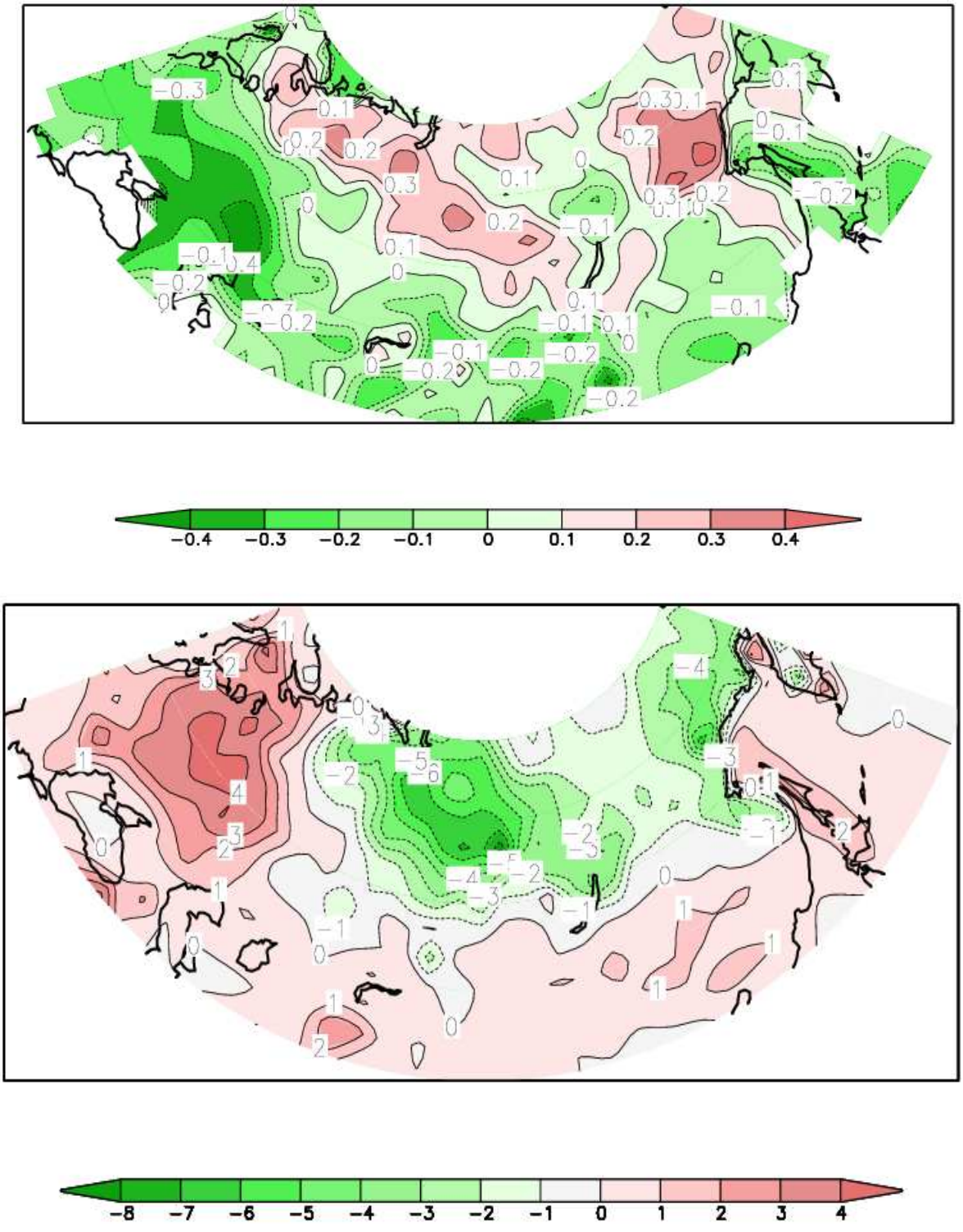

Figure 6: (a) Correlation coefficients between DJF Eurasian snow depth anomalies with the following ISMR anomalies during 1961-1990 and (b) EOF-1(13%) of DJF snow depth during 1961-1990.

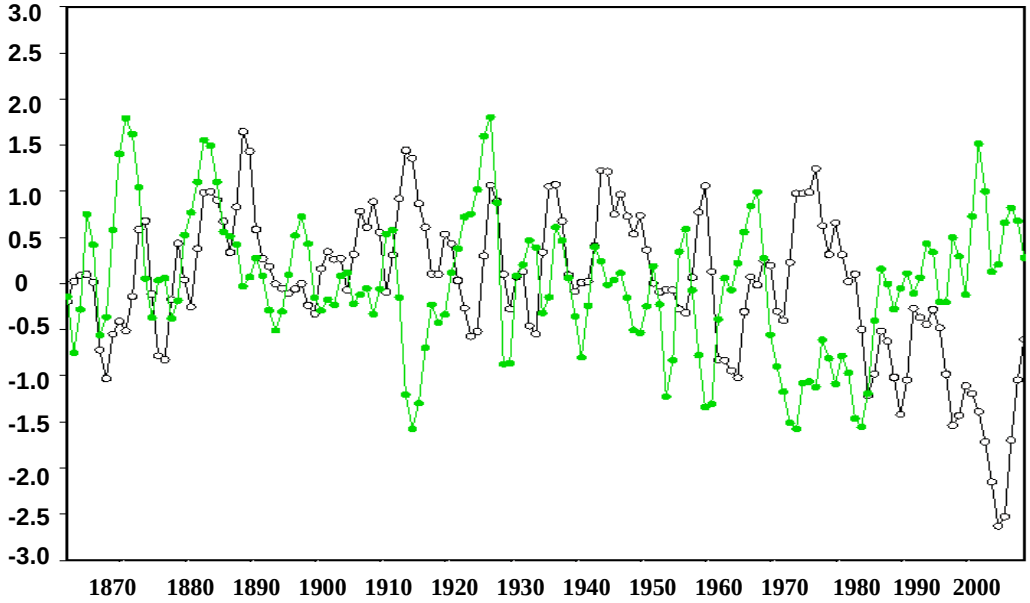

Figure 7: Standardized DJF snow depth anomalies over western Eurasia (open circles) and ISMR anomalies (closed circles) during 1861–2008.

1
2

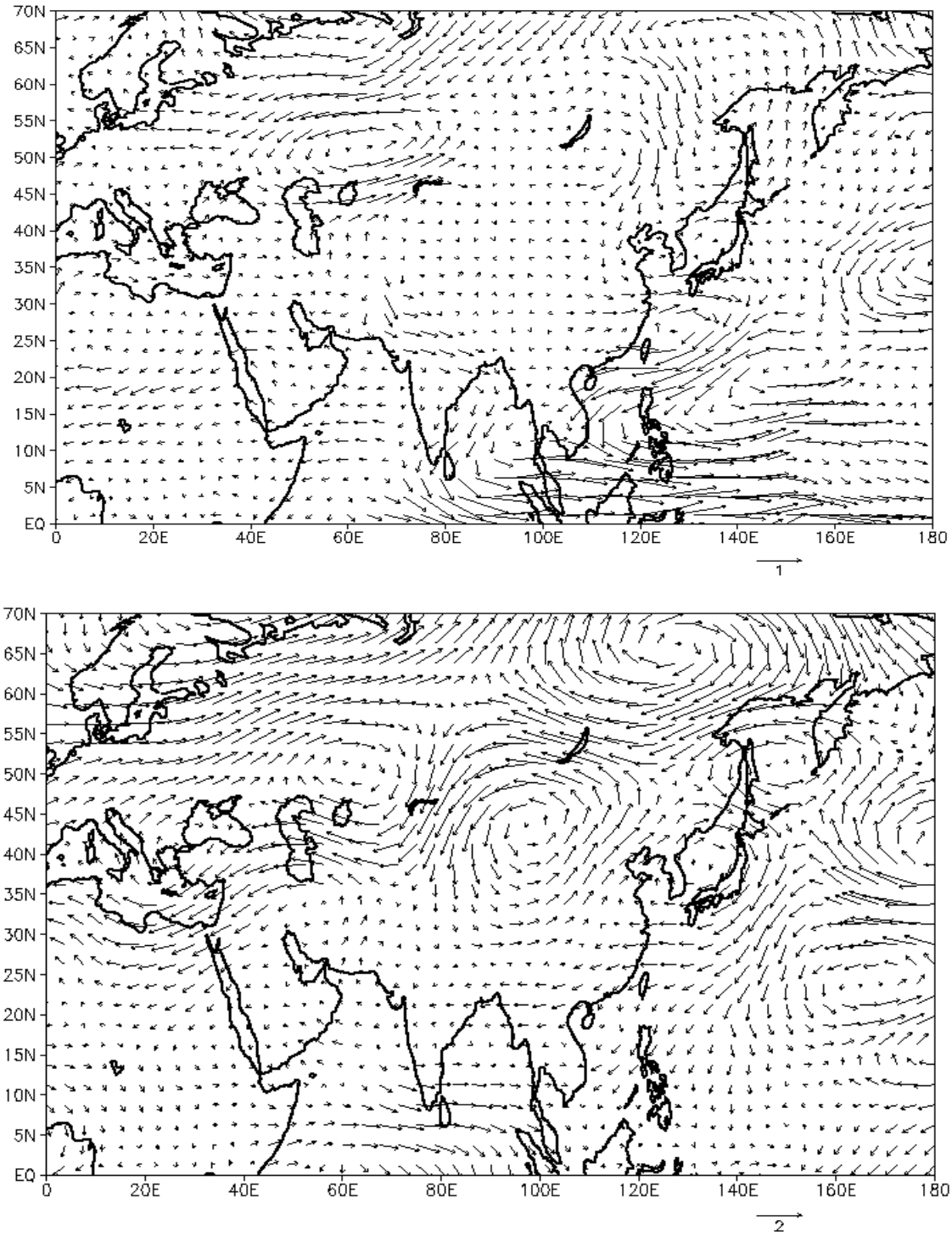

Figure 8: Wind differences (m/s) between the composites of high and low snow years at (a) 850 hPa level and (b) 200 hPa.

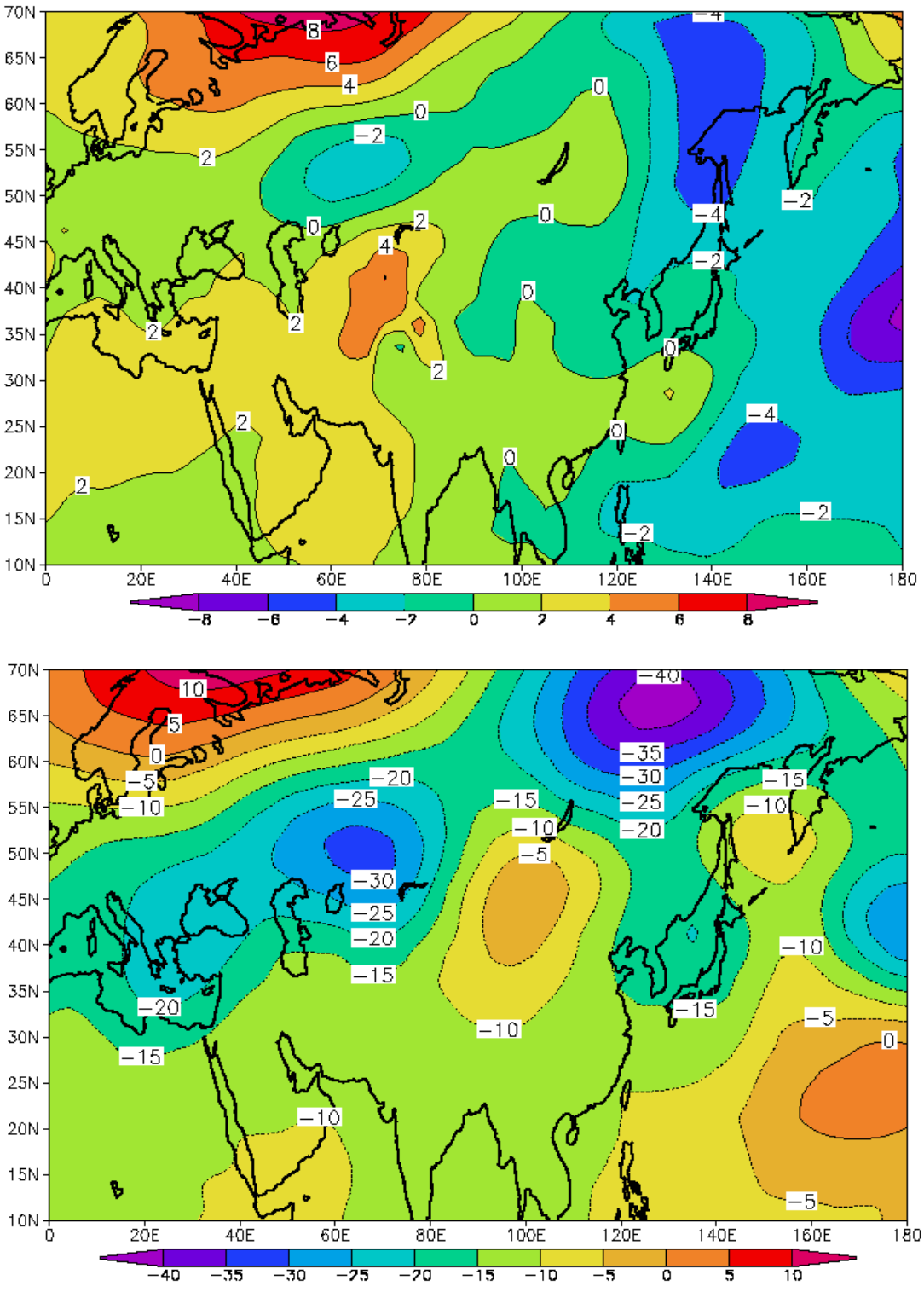

(a)

(b)

Figure 9: Geopotential height differences (m) between composites of high and low snow years at (a) 850 hPa level and (b) 200 hPa.

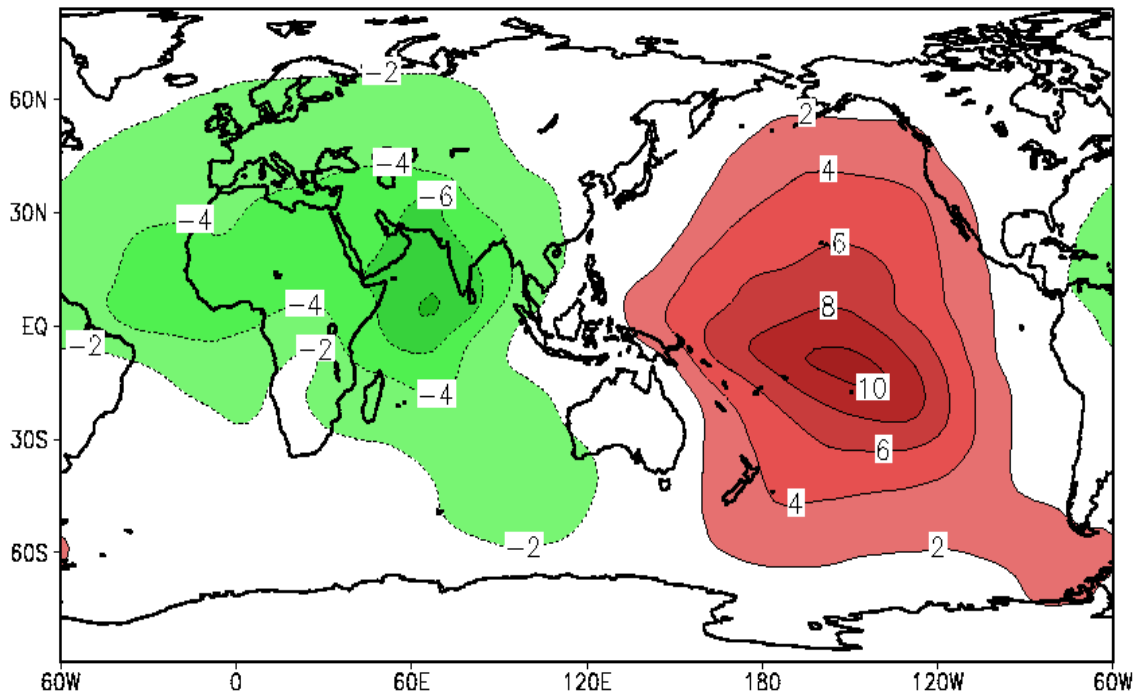

(a)

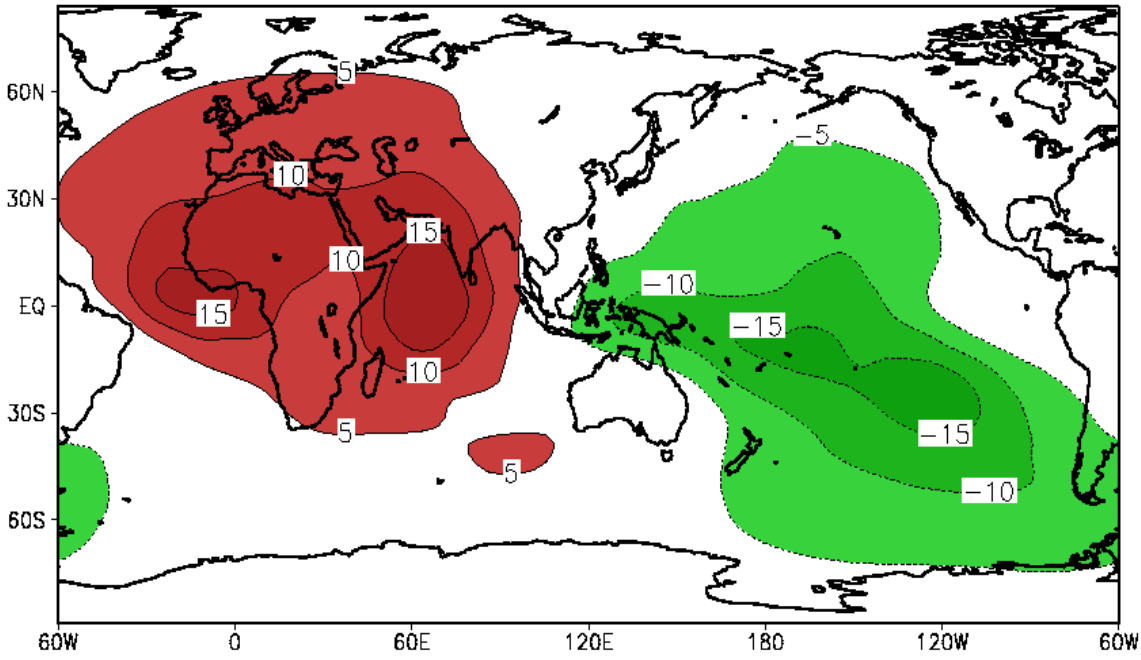

(b)

Figure 10: Velocity potential (χ) differences (m^2/s) between composites of high and low snow years at (a) 850 hPa and (b) 200 hPa.

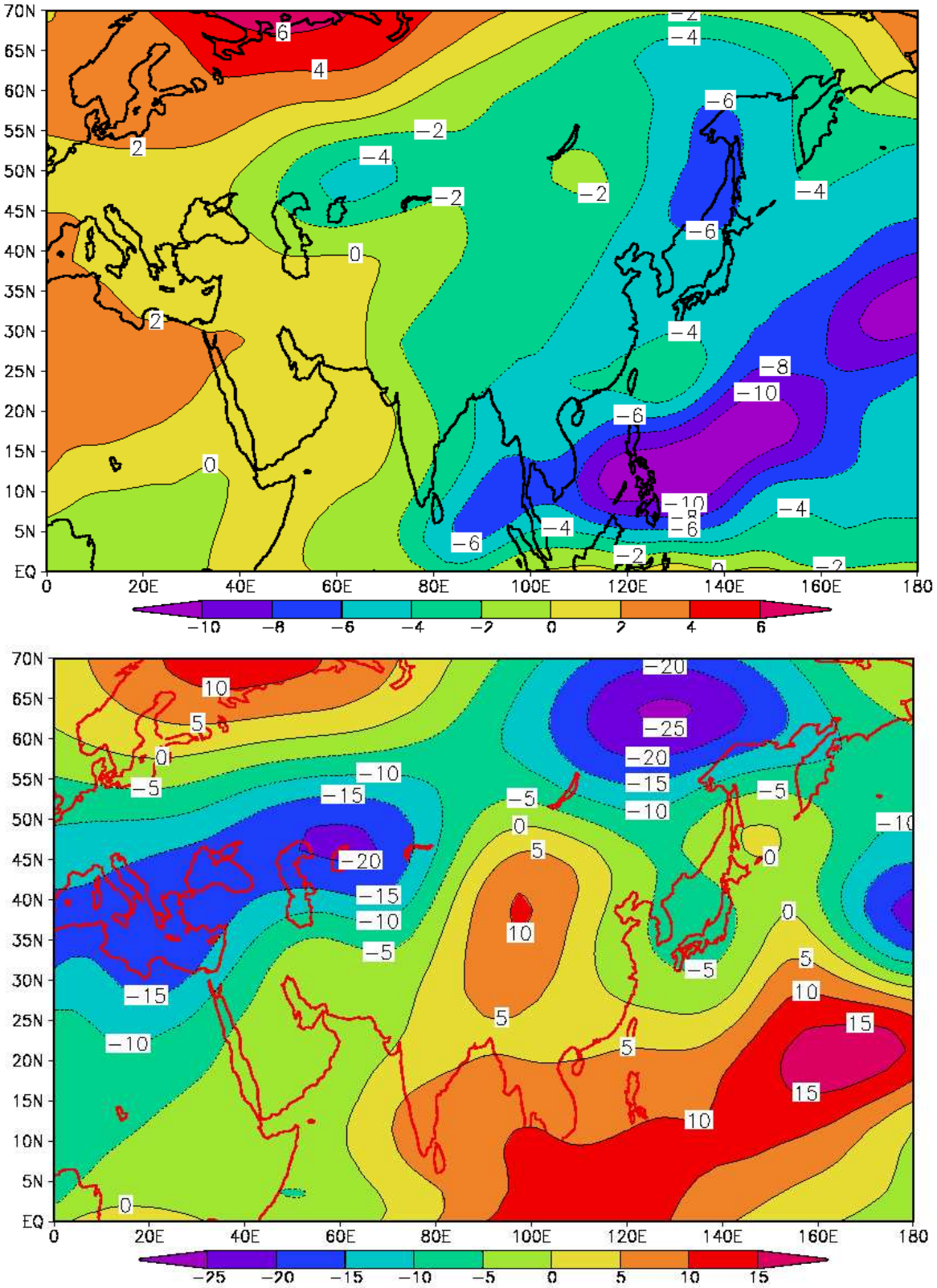

(a)

(b)

Figure 11: Stream function differences (m^2/s) between composites of high and low snow years at (a) 850 hPa and (b) 200 hPa.